Supporting Information for "Solar Wind Protons forming Partial Ring Distributions at Comet 67P"

A. Moeslinger[1,2], G. Stenberg Wieser[1], H. Nilsson[1], H. Gunell[2], H.N. Williamson[1], K. LLera[3], E. Odelstad[4], I. Richter[5]

[1]Swedish Institute of Space Physics, 981 28 Kiruna, Sweden

[2]Department of Physics, Umeå University, 901 87 Umeå, Sweden

[3]Southwest Research Institute, San Antonio, TX, USA

[4]Swedish Institute of Space Physics, 75121 Uppsala, Sweden

[5]Institut für Geophysik und extraterrestrische Physik, Technische Universität Braunschweig, 38106 Braunschweig, Germany

Contents of this file

Introduction

This supporting information contains an additional angular plot with a dual colourmap for the reference case (figure S1). An overview plot of the spacecraft position in magnetic field coordinates is given in figure S2. Figure S3 is an example figure for the dual colourmap used for figures 3, 4, and 5 in the main text. Field-of-view obstructions of ICA and IES are shown in figure S4.

Figure S1. Reference case - Angular plots

Figure S1 shows the angular distribution of protons and alpha particles as measured by ICA during our reference case (April 23rd, 2016, at 11:32). The lower median energy of the protons could be due to a slower upstream solar wind, or due to a higher electrostatic potential difference from the observation point to the upstream solar wind. As the alpha particles are also observed at much lower energies, the dominating influence seems to be the upstream solar wind conditions (Nilsson et al., 2022). The signal to the left in the upper panel is an instrumental effect (cross-talk) and not a real signal.

Figure S2. Spacecraft position in magnetic field coordinates

To define the magnetic / electric field coordinate system we aligned the x-axis with the sunward direction as an approximation for the negative upstream solar wind flow direction. For the y-axis, which is usually aligned along the magnetic field component perpendicular to the velocity in this coordinate frame, we used the local magnetic field measured by MAG for both cases (see green markers in figure S2). Additionally, we also used the estimated ring parameter $\mathbf{u}_{bulk,\parallel}$ to provide an alternative estimate of the magnetic field direction. The results of using the component of $\mathbf{u}_{bulk,\parallel}$ perpendicular to the x-axis is shown with red markers in figure S2. The z-axis completes the right-hand system and is along the convective electric field ($\mathbf{E} = -\mathbf{v} \times \mathbf{B}$). The $+E$- and $-E$- hemispheres are found at $z > 0$ and $z < 0$. In panel a), the dataset using the MAG measurements is rescaled by 0.8 to avoid overlap between the datapoints.

On both days the majority of data points are at $z > 0$, but the spread is significant, especially for the partial rings case when using the local magnetic field measurements.

Using the $\mathbf{u}_{bulk,\parallel}$ estimate instead of the MAG measurements significantly reduces the spread to about half of the angular variation.

Figure S3. Dual Colourmap Example

Figure S3 shows how a change in energy or differential flux affects the dual colourmap plots. In the two panels at the top, the energy is fixed at 500 eV and 1000 eV. The differential flux is varied over the entire range of the colourmap. The bottom three panels show the reversed case, where the energy varies but the differential flux is kept constant. The range and settings of the dual colourmap are identical to the ones used in the main text.

Figure S4. ICA and IES Field-of-View obstruction

The nominal pixel layout and field-of-view (FoV) of the two ion spectrometers ICA and IES are shown in figure S4. Both FoVs are given in ICA instrument coordinates for easier comparison between the two panels. The distortion of the IES FoV is due to the rotation that is required to transform it into ICA instrument coordinates. The narrow-gridded area in the IES pixel layout is the high-resolution sector (binned in the data used for this study). In both panels, the obstruction in the FoV is shown by the grey areas. These obstructions are due to shadowing of the spacecraft and one of the solar arrays, as well as the High Gain Antenna in the case of IES. The shadowed areas of the two instruments are slightly different because of their different mounting position. Ions arriving from the shadowed directions cannot be observed by the instrument. A more detailed analysis of the IES FoV obstructions can be found in Clark et al. (2015).

References

Clark, G., Broiles, T. W., Burch, J. L., Collinson, G. A., Cravens, T., Frahm, R. A.,

... Pollock, C. J. (2015, 11). Suprathermal electron environment of comet 67p/churyumov-gerasimenko: Observations from the rosetta ion and electron sensor. *Astronomy and Astrophysics*, *583*. doi: 10.1051/0004-6361/201526351

Nilsson, H., Moeslinger, A., Williamson, H. N., Bergman, S., Gunell, H., Wieser, G. S., ... Holmström, M. (2022, 3). Upstream solar wind speed at comet 67p: Reconstruction method, model comparison, and results. *Astronomy and Astrophysics*, *659*. doi: 10.1051/0004-6361/202142867

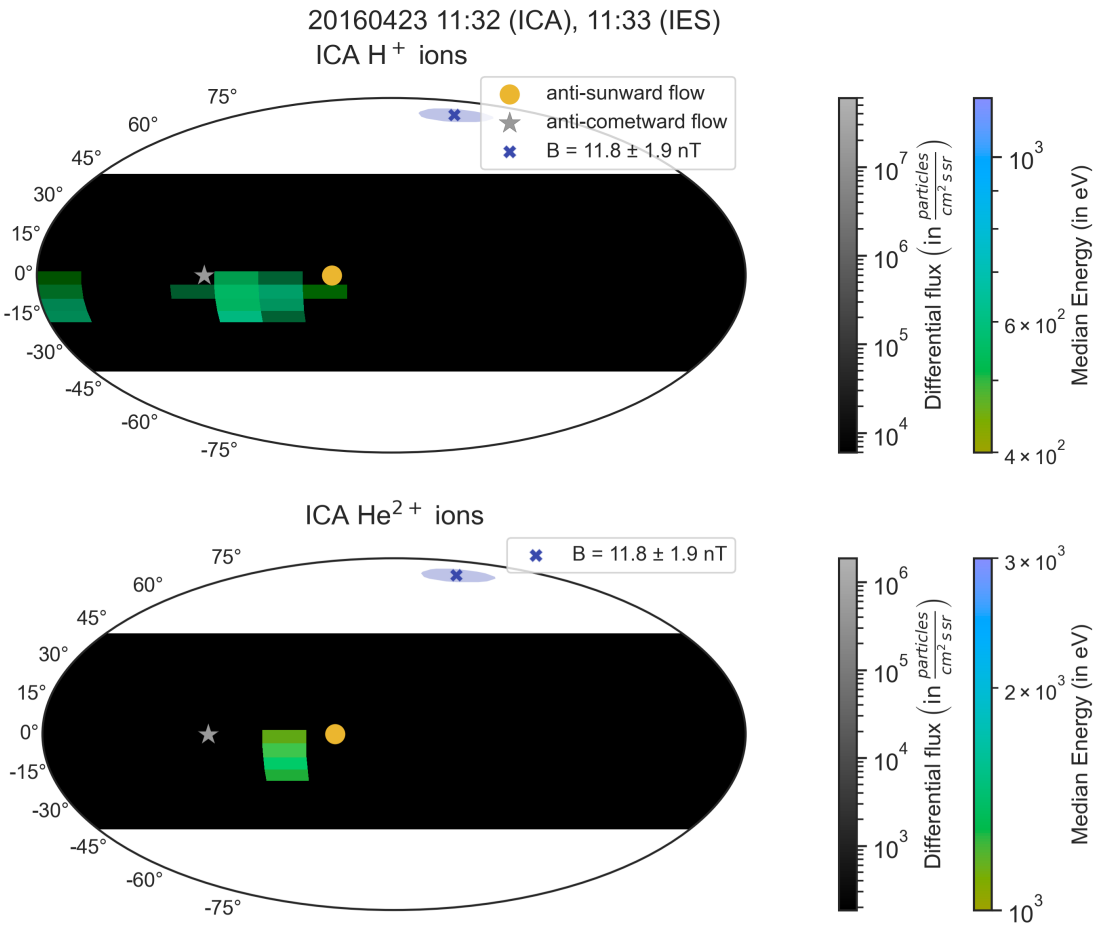

Figure S1. Azimuth - Elevation plots of a single scan during our reference case (April 23rd, 2016, at 11:32). The format is the same as in figure 5 in the main text, but no ring fits are shown.

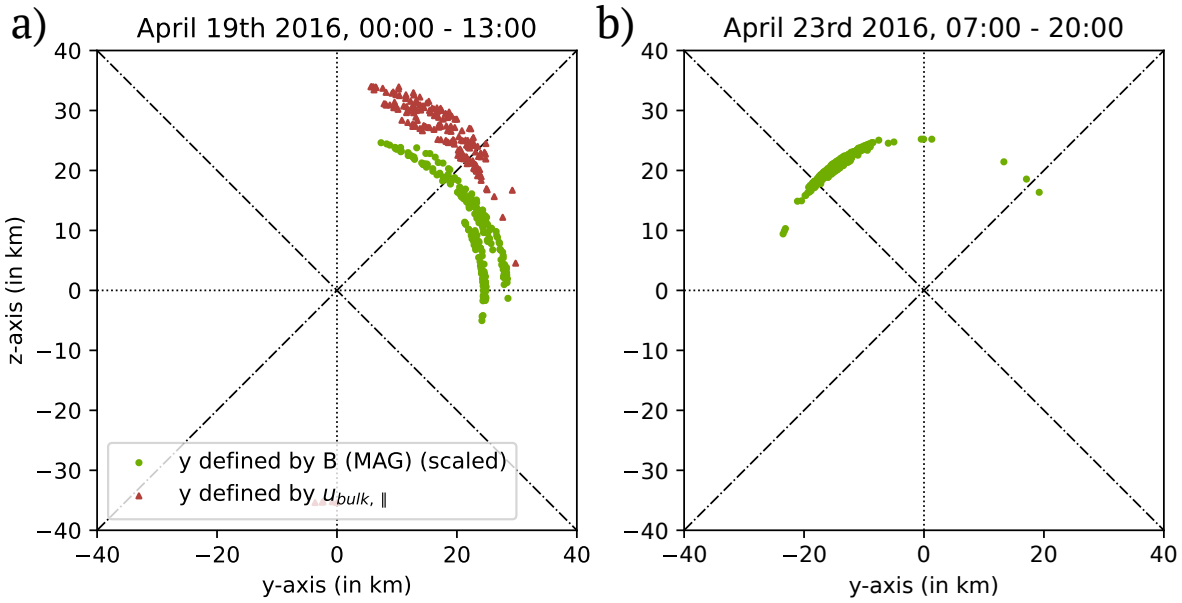

Figure S2. Spacecraft position in magnetic field coordinates projected into the y-z plane. Panel a) shows data for our main case with partial rings, and panel b) for the reference case.

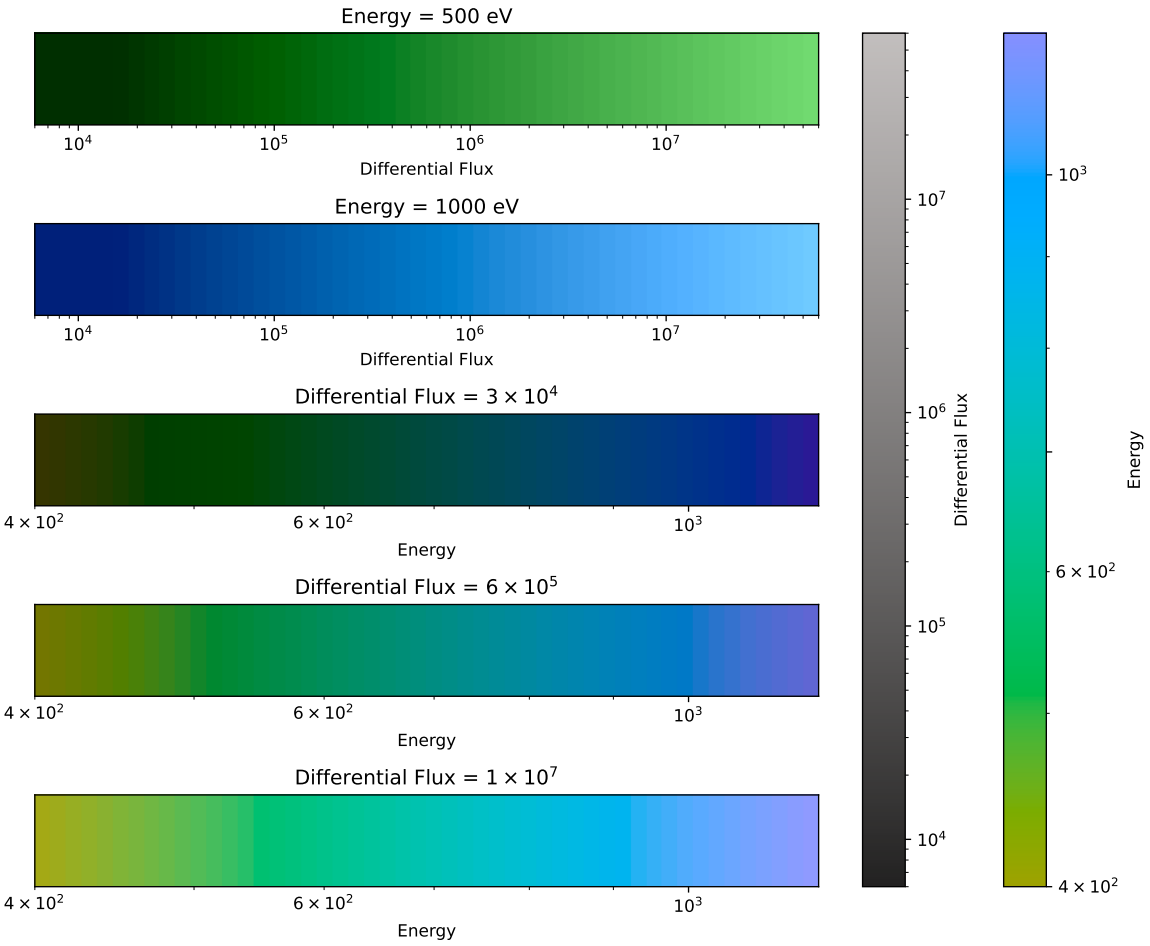

Figure S3. Dual colourmap variable illustration. The top two panels show the effect of a changing differential flux for a constant energy. In the bottom three panels, the influence of a changing energy at a constant differential flux is shown.

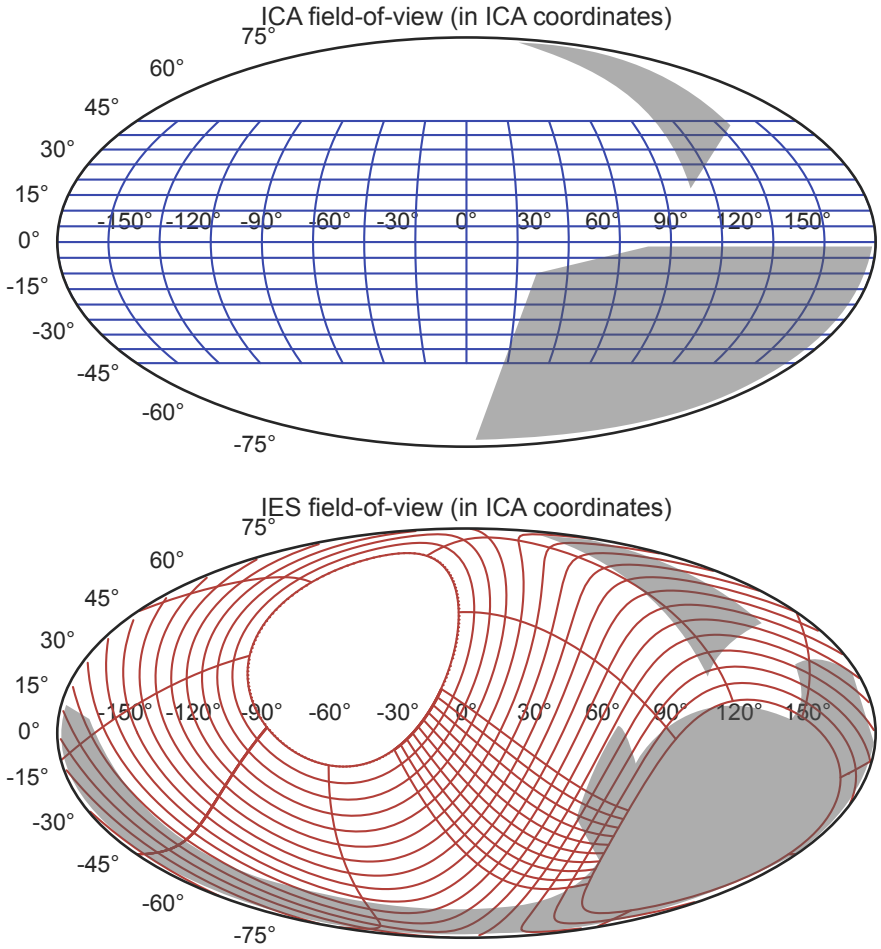

Figure S4. ICA (top panel) and IES (bottom panel) field-of-view, rotated into ICA instrument coordinates. The grid lines indicate the individual instrument pixels. The grey areas show obstructions in the field-of-view of the respective instrument due to spacecraft blockage.